Journal of Physics D:
Applied Physics

PURPOSE-LED
PUBLISHING™

PAPER

Random telegraph signal generation based on magnetic tunnel junction for security and unconventional computing applications

To cite this article: Jiajia Jian *et al* 2026 *J. Phys. D: Appl. Phys.* **59** 015005

View the article online for updates and enhancements.

You may also like

- Biomolecular mass spectrometry in plasma medicine
Zengyu Wang, Klaus-Dieter Weltmann, Sander Bekeschus et al.
- Relative stabilities and physical parameters of rhombohedral distorted HfO_2 crystalline phases
Yun-Wen Chen and C W Liu
- Role of self-healing on defects generation and nitrogen incorporation in graphene exposed to diffuse dielectric barrier discharge in N_2
C Moderie, P Vinchon, R Martel et al.

This content was downloaded from IP address 123.138.191.162 on 24/03/2026 at 01:43

Journal of Physics D: Applied Physics

Check for updates

RECEIVED
24 June 2025

REVISED
27 October 2025

ACCEPTED FOR PUBLICATION
10 December 2025

PUBLISHED
4 March 2026

PAPER

Random telegraph signal generation based on magnetic tunnel junction for security and unconventional computing applications

Jiajia Jian[1,6], **Xihui Yuan**[1,2,6], **Fangyi Zhao**[1], **Zheng Chai**[1,*], **Xue Zhou**[1], **Yongjie Luo**[1], **Xin Yue**[1], **Jian Fu Zhang**[5], **Weidong Zhang**[3] and **Tai Min**[1,4,*]

[1] The Center for Spintronic and Quantum Systems, State Key Laboratory for Mechanical Behavior of Materials, and School of Materials Science and Engineering, Xi'an Jiaotong University, Xi'an 710049, People's Republic of China
[2] School of Microelectronics, Xidian University, Xi'an, 710126, China, and also with Hangzhou Institute of Technology, Xidian University, Hangzhou 311200, People's Republic of China
[3] School of Engineering, Liverpool John Moores University, Liverpool, L3 3AF, United Kingdom
[4] School of Functional Materials and Intelligent Manufacturing, Nanjing University, Suzhou, 215163, People's Republic of China
[5] Current address: School of Integrated Circuits, Southeast University, Nanjing 210096, People's Republic of China.
[6] Authors with equal contribution.
[*] Authors to whom any correspondence should be addressed.

E-mail: zheng.chai@xjtu.edu.cn and tai.min@nju.edu.cn

Keywords: magnetic tunnel junction, random telegraph signal, stochastic computing, artificial neural network

Abstract

Random telegraph signals (RTS) can serve as a physical entropy source for hardware security, stochastic computing, and artificial intelligence, yet the conventional implementations of RTS face critical limitations: CMOS-based approaches suffer from area inefficiency; emerging memristors offer probabilistic switching but lack controllability; while existing spintronic RTS solutions require external magnetic fields with limited tunability. This work introduces a field-free, electronically modulated RTS methodology using a single magnetic tunnel junction. By exploiting voltage-controlled stochastic magnetization switching, we generate intrinsically random RTS with demonstrated cryptographic-grade randomness. The RTS platform successfully executes key exchange protocols and real-time voice encryption. Crucially, the core parameters of RTS—state occupation ratio and transition time constants—can be dynamically modulated via excitation amplitude adjustment. This controllable RTS also successfully achieved image edge detection without post-processing and played a significant role in suppressing overfitting of neural networks. This voltage-modulated RTS paradigm bridges hardware stochasticity with algorithmic demands, establishing a robust foundation for secure and efficient computing systems.

1. Introduction

Random telegraph signals (RTS), characterized by random fluctuations between discrete voltage or current levels [1], represent a promising physical entropy. Their inherent randomness, low energy consumption, and minimal transistor footprint make them highly attractive for critical applications such as hardware security [2], unconventional computing paradigms [3, 4], and artificial intelligence [5].

Among naturally occurring RTS, random telegraph noise (RTN) stands as a widely reported example [6, 7]. RTN arises from the stochastic trapping and detrapping of charge carriers at oxide defects within nanoscale semiconductor devices, including MOSFETs [8, 9]. This phenomenon plays a vital role in several potential and promising applications, including true random number generators (TRNGs) [10–12], neuromorphic computing [13], physical unclonable functions (PUFs) [14], and temperature sensors [15].

However, the practical utilization of naturally occurring RTN faces fundamental challenges. The random spatial distribution of defects makes RTN inherently scarce and unpredictable in standard CMOS devices. Harvesting usable RTN signals necessitates laborious screening of large device arrays, often requiring sophisticated algorithms or manual characterization [16, 17]. Furthermore, RTN's capture and emission time constants (τ_c and τ_e, respectively)—critical parameters for RTN-based systems—exhibit

© 2026 IOP Publishing Ltd. All rights, including for text and data mining, AI training, and similar technologies, are reserved.

pronounced sensitivity to process, voltage, and temperature variations [18, 19] that degrade application performance. While approaches like electrical stress or dedicated AC operation have been proposed to enhance RTN occurrence or robustness [20], they inevitably increase power consumption and complexity without fully resolving the core issue of reliance on stochastic defects.

To overcome these limitations of defect-dependent natural RTS, research has shifted towards artificially generating controllable RTS instead of finding RTN from the device. Emerging devices with probabilistic switching characteristics (such as memristors [21, 22]) are attractive for this task. Unlike CMOS technology, the storage mechanism of these novel memories relies on resistance changes to achieve different logical states [23]. Due to the specific physical architecture, theses emerging devices can provide an intrinsic ultra-small entropy source and have the potential to be a new technology for RTS generation.

In this context, magnetic random-access memory (MRAM) emerges as a particularly promising platform [24, 25] due to its fast switching, exceptional endurance, inherent stability, and low power consumption [26]. Indeed, magnetic tunnel junctions (MTJs) have emerged as versatile platforms for TRNG, leveraging diverse mechanisms including superparamagnetic switching [27–29], voltage-controlled magnetic anisotropy [30, 31], and spin–orbit torque [32, 33]. These methods exploit thermal fluctuations to harvest randomness, often achieving high-speed, low-power entropy generation.

Among them, low-barrier MTJs with controllable switching probability have been developed, but it requires special processes [34] and is different from MRAM used for memory applications. And they cannot control the time each state stays in individually. Besides, existing RTS generation schemes based on MRAM typically require the application of both electrical pulses and external magnetic fields [35, 36], which complicates integration with commercial integrated circuits. In addition, the generated RTS is only marginally tunable under variable externally applied magnetic fields, further limiting its practical applications due to limited adaptability.

This paper addresses these critical challenges by proposing a novel method for generating tunable spintronic RTS. Our approach operates exclusively within a single MRAM device and relies solely on electronic operations, eliminating the need for external magnetic fields. We demonstrate that the generated RTS exhibits excellent randomness, validating its efficacy in demanding applications like encryption (including key exchange and real-time voice encryption). Crucially, we show that key RTS parameters—namely the state occupation ratio and time constants—can be precisely modulated by simply varying the amplitude of the applied electrical waveform. This inherent controllability paves the way for efficient deployment in random computing and neuromorphic networks, offering a robust, integrable, and energy-efficient entropy source that overcomes the fundamental drawbacks of both natural RTN and existing artificial generation methods.

2. Experimental methods

In this study, we utilize spin transfer torque MRAM (STT-MRAM) as the device for generating spintronic RTS. The core storage element of the STT-MRAM consists of a bottom-pinned perpendicular magnetic anisotropy (PMA) MTJ. Figure 1(a) presents a cross-sectional schematic and structural diagram of the MTJ with a diameter of ∼70 nm and $\Delta = 80$ at 298.15 K used in this work. All electrical measurements were performed using pulse measurement units in a Keithley 4200 semiconductor characterization system.

3. Results and discussion

3.1. RTS generator based on MTJ

The switching process of the MTJ is governed by the combined effects of STT and thermal fluctuations. *R–V* curve and *R–H* curve (figure 1(b)) shows the magneto-resistive switching between the low resistance (P) state and the high resistance (AP) state, as the industrial-ready device is thermally stable. As shown in figure 1(c), upon application of a positive voltage (V_+), STT-driven alignment induces anti-parallel magnetization between the free and pinned layers, establishing a high-resistance state (AP). Conversely, under V^- bias, parallel alignment is energetically stabilized, transitioning the device to a low-resistance state (P). Thermal fluctuations introduce stochasticity into the switching dynamics, enabling probabilistic state transitions, which behaves stochastic switching at applied voltages below the critical threshold. The stochastic switching of MTJ device can be explained by the Néel–Brown in equation (1) and (2),

$$P(t) = 1 - \exp(-t/\tau) \tag{1}$$

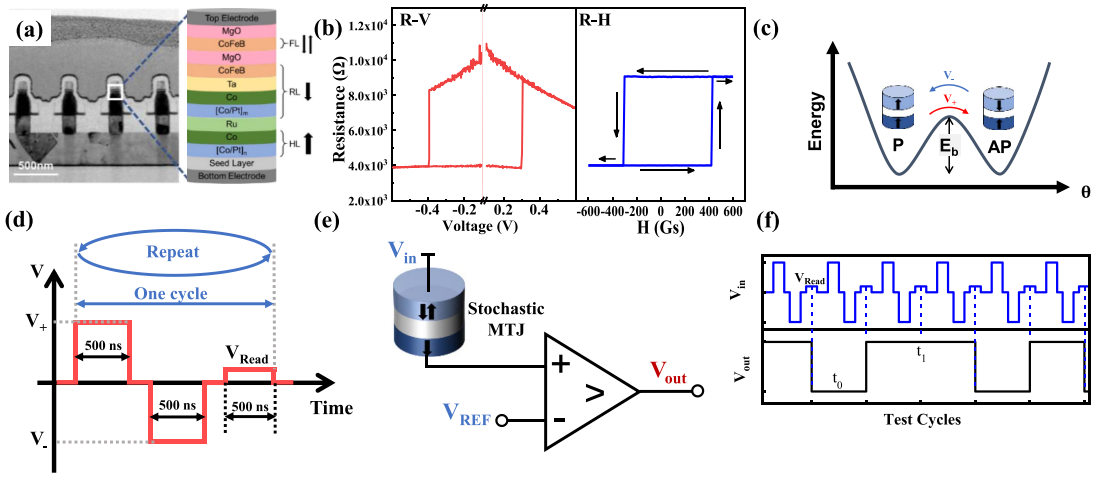

Figure 1. Schematic of the random telegraphy signal generation method based on MTJ with a diameter of ∼70 nm. (a) Cross section scanning electron microscope (SEM) and structure demonstration of MTJ. (b) *R–V* and *R–H* curves show the magnetic-resistive switching of two MTJs with two stable states. (c) Schematic diagram of the switching mechanism of MTJ. (d) The designed three-stage combined pulse waveform includes V_+, V_- and V_{read}. (e) Circuit diagram of RTS generator based on MTJ. (f) Input–output voltage relationship ($V_{in} \leftrightarrow V_{out}$) in the proposed RTS generator circuit.

where $P(t)$ is the thermal switching probability, and τ is the relaxation time,

$$\tau = f_0^{-1} \exp\left(E_b / k_B T\right) \tag{2}$$

where f_0 is the attempt frequency, E_b is the energy barrier, and T is the temperature.

Accordingly, a composite pulse waveform was designed in figure 1(d), comprising three functional phases: A positive-voltage pulse (V_+) inducing probabilistic switching from the parallel (P) to antiparallel (AP) state; A negative-voltage pulse (V_-) driving reverse magnetization switching; A measurement pulse sampling the MTJ resistance state. The bipolar voltage pulses have been previously explored to induce stochastic MTJ switching [37] used this waveform to model the switching process via Markov chains and then solve a linear algebra problem [38]. By contrast, this work transforms the underlying physical mechanism into a programmable entropy source, generating an intrinsic RTS that enables broader application. This opposing-polarity excitation induces stochastic oscillation between P and AP states, yielding an intrinsic RTS. An RTS generator is proposed in figure 1(e), comprising two core components: stochastic MTJ unit and a comparator circuit. V_{in} inputs a combined pulse waveform, then MTJ generates RTS randomly after receiving the stimulus. The RTS is read and compared with the reference value to generate digital RTS sequence. When the MTJ assumes an AP state, the digital output signal corresponds to logic level '1'; conversely, a P state yields logic level '0' The RTSs shown in this article were generated at a sampling rate of 0.28 MHz and a duty cycle of 0.43. It is worth noting that the sampling rate can be as high as 100 MHz or more due to the ultra-fast switching of the MTJ [39], which is orders of magnitude faster than the existing MTJ-based superparamagnetic oscillation in milliseconds [40].

Figure 1(f) illustrates the temporal relationship between input stimulus and output bits. Each comparison cycle produces one random bit, with V_{ref} and V_{in} maintained constant throughout repeated cycles to generate a digital bit stream of any length. In the proposed MTJ-based RTS, the durations of continuous P and AP states are denoted as t_0 and t_1, respectively, with $\tau 0$ and $\tau 1$ denoting their corresponding averages—both critical parameters for RTS in equation (3). Herein, the 'duration' refers to the number of consecutive identical bits,

$$\tau_x = \frac{1}{N_x} \sum t_x \tag{3}$$

where t_x is the ith dwell time for state x, and N_x is the total number of segments observed in that state.

3.2. Randomness evaluation

Under pulse amplitude of $V_+ = 280$ mV, $V_- = -340$ mV, all with a pulse width of 500 ns, a 200 000-bit digital RTS was generated, with figure 2(a) depicting an exemplary segment of this sequence. Theoretically, RTSs—including RTN, stochastic switching in ovonic threshold selectors [41], and

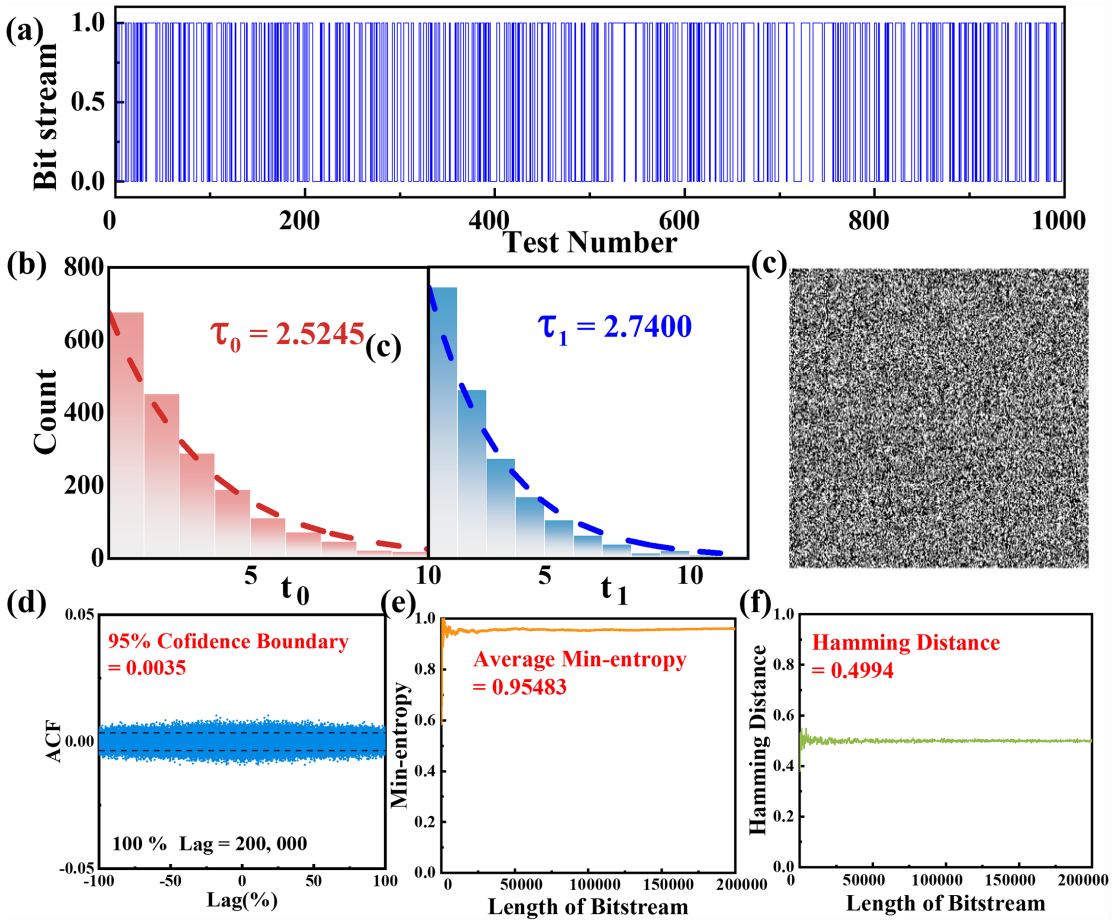

Figure 2. Statistical randomness characterization of MTJ-generated digital RTS (a) demonstration of digital RTS sequence generated at $V_+ = 280$ mV and $V_- = -340$ mV, all with a pulse width of 500 ns. (b) The t_0 and t_1 all follow the exponential distribution. (c) Bit map. (d) Autocorrelation function analysis. (e) Minimum entropy evaluation. (f) Hamming distance.

stochastic magnetic oscillators [4]—conform to Poisson processes, where inter-state transition intervals follow an exponential distribution. Experimentally, as evidenced by the exponential distributions of t_0 and t_1 in figure 2(b), the generated spintronic RTS in figure 2(a) exhibits Poissonian statistics consistent with this theoretical framework.

Statistical tests are conducted to evaluate the randomness quality of the generated bitstream. Figure 2(c) presents the bit distribution map, where logical 1 and 0 states are represented by black and white units. They account for 51% and 49% of the total sequence respectively. The absence of any discernible pattern supports the good randomness of the RTS.

Figure 2(d) shows the relative autocorrelation scatter plot of the generated random numbers, and the 95% boundary (95% confidence interval, 95% CI) of the relative autocorrelation is 0.0035, indicating that the generated random numbers have low autocorrelation and good randomness. Entropy is a measure of the uncertainty of a random sequence. The average entropy of the generated random number sequence is 0.954 83 in figure 2(e), indicating excellent unpredictability. In addition, hamming distance (HD) is employed to determine the dissimilarity between two equal-length signals from original RTS. Figure 2(f) shows that the HD is 0.4994 when the length of bitstream is 200 000, which further shows that the generated random numbers are evenly distributed and have good unbiasedness.

3.3. Applications of RTS generator

3.3.1. RTS generator for cryptographic applications

Random signals intended for cryptographic applications need satisfy more stringent requirements than those for general purposes, including uniform statistical independence, unpredictability, and absence of discernible patterns. The NIST Statistical Test Suite (NIST) evaluates these critical characteristics. As evidenced by figure 3(a), the generated true random sequence successfully passed all 12 statistical tests in the NIST SP 800–22 standard, validating its suitability for cryptographic implementations.

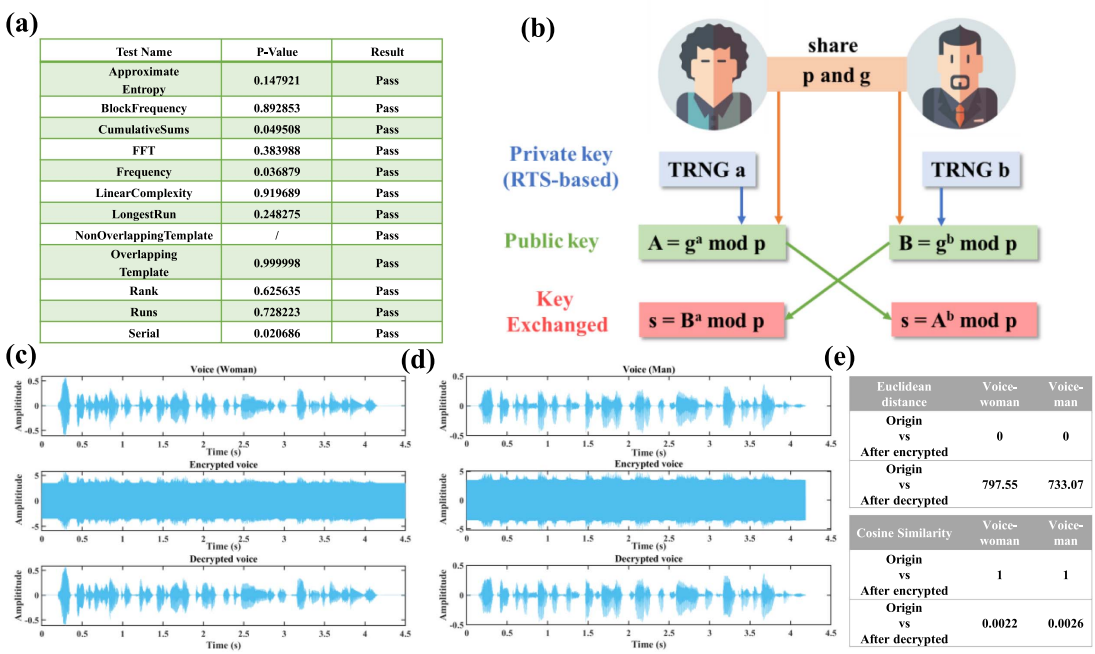

Test Name	P-Value	Result
Approximate Entropy	0.147921	Pass
BlockFrequency	0.892853	Pass
CumulativeSums	0.049508	Pass
FFT	0.383988	Pass
Frequency	0.036879	Pass
LinearComplexity	0.919689	Pass
LongestRun	0.248275	Pass
NonOverlappingTemplate	/	Pass
Overlapping Template	0.999998	Pass
Rank	0.625635	Pass
Runs	0.728223	Pass
Serial	0.020686	Pass

Euclidean distance	Voice-woman	Voice-man
Origin vs After encrypted	0	0
Origin vs After decrypted	797.55	733.07

Cosine Similarity	Voice-woman	Voice-man
Origin vs After encrypted	1	1
Origin vs After decrypted	0.0022	0.0026

Figure 3. Demonstration of RTS generator in security applications. (a) 12 NIST test results of the digital RTS bitstream generated under generated at $V_+ = 280$ mV and $V_- = -340$ mV. (b) Schematic diagram of the D–H protocol flow based on RTS generator. (c) Encryption and decryption audio of female and (d) male voices. (e) Euclidean distance and cosine similarity were utilized to evaluate the performance.

The proposed RTS generator can be used for cryptographic implementations in both digital and analog domains. An RTS generator based Diffie–Hellman (D–H) Key Exchange protocol is demonstrated in figure 3(b) in a digital form. D–H key exchange allows two communicating parties to create a shared secret key over an insecure channel. Both parties only share p and g, obtain their own random private keys through RTS generator, and obtain a shared private key through calculation after transmitting information in the public channel.

The cryptographic application of analog signals is validated through speech encryption/decryption. As shown in figures 3(c) and (d), a symmetric algorithm [42] employs male and female audio signals as validation benchmarks. The encryption process implements equation (4), while decryption executes equation (5),

$$x(n)_d = \frac{\frac{x(n)-RTS_5}{RTS_4} - RTS_1}{RTS_2} + RTS_3 \tag{4}$$

$$x(n) = \left(\left(\left(x(n)_d - RTS_3\right) * \left(RTS_2\right)\right) + RTS_1\right) * RTS_4 + RTS_5. \tag{5}$$

The input signal $x(n)$ represents an audio sequence containing the text: 'Welcome to the center for spintronic materials and quantum devices.' Encryption employs five distinct random sequences (RTS_1–RTS_5) generated by original RTS and $x(n)_d$ represents the encrypted speech sequence. Despite spectral disparities between male and female vocal inputs, both signal types exhibit effective encryption, manifested that original content auditorily unrecognizable. And lossless decryption is confirmed by waveform reconstruction. These results collectively validate the cryptographic robustness of the proposed RTS generator for digital and analog security applications. To quantitatively validate the audio encryption/-decryption process, we compared vectorized representations of the original, encrypted, and decrypted signals (figure 3(e)). Euclidean distance analysis confirms strong encryption distortion. The original-to-encrypted distance approaches zero, while the original-to-decrypted distance is significant—indicating effective restoration [43]. Complementary cosine similarity metrics) further verify this behavior. The encrypted signal shows near-orthogonality to the original (value ≈1, denoting minimal overlap), while the decrypted signal exhibits extremely low similarity to its encrypted counterpart [44]. Together, these results demonstrate both effective encryption and precise waveform recovery.

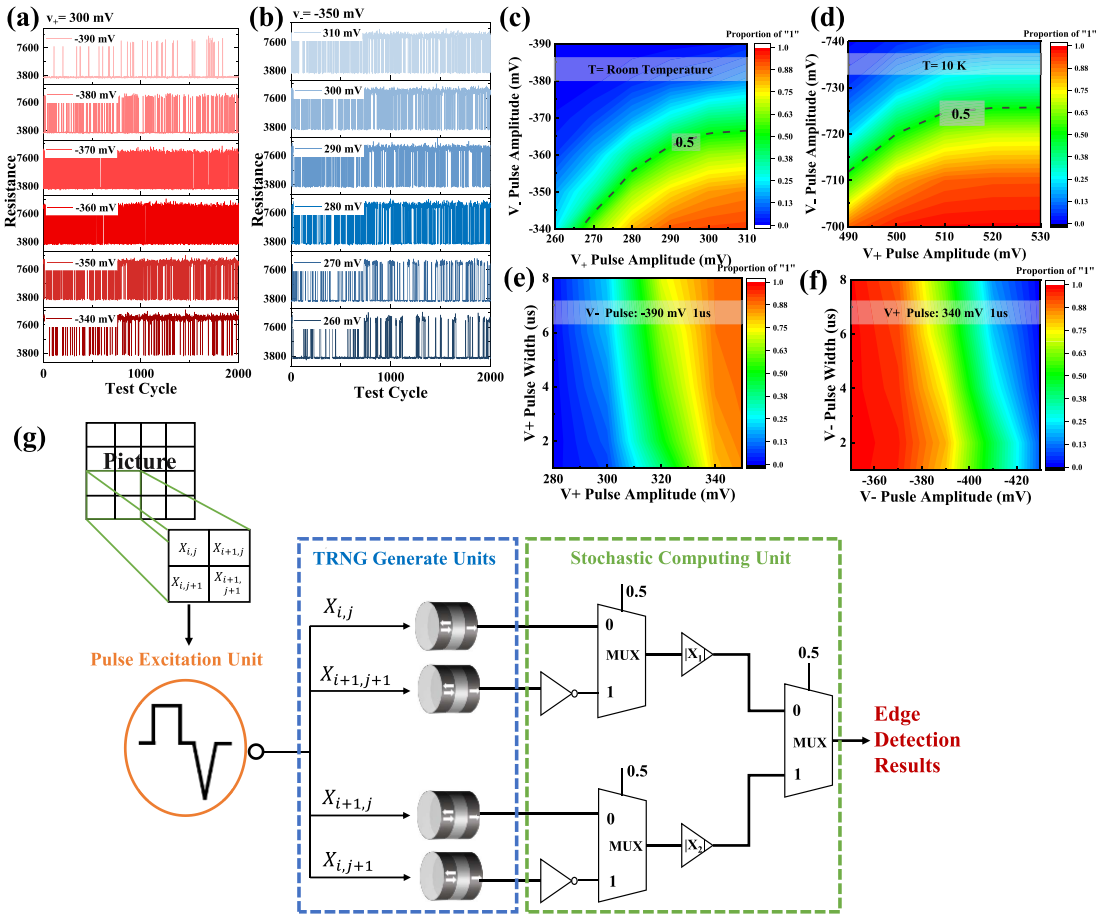

Figure 4. Demonstration of RTS generator in novel computing. V_+ (a) and V_- (b) regulate the ratio of two states in the sequence. Heat map of the relationship between voltage amplitude and the proportion of '1' in the sequence at (c) T = room temperature and (d) $T = 10$ K, respectively. Dependence of '1' s proportion on (e) the V_+ pulses amplitude and pulse width at fixed V_- pulse and (f) the V_- pulses amplitude and pulse width at fixed V_+ pulse. (g) Hardware architecture of random computing edge detection implemented using RTS generator based on MTJ.

3.3.2. RTS generator for stochastic computing

It is also hoped that RTS can show good controllability. Given that V_+ and V^- respectively govern stochastic switching in opposite MTJ magnetization orientations, the probability distribution of output bits (0/1 ratio) becomes tunable through excitation amplitude modulation. As figure 4(a) demonstrates, increasing V_+ elevates the probability of state 1 occurrence, while figure 4(b) reveals an inverse relationship where V^- reduces this probability. These voltage parameters enable control over both temporal characteristics and state offers significant advantages for emerging computational paradigms—particularly stochastic computing (SC). In SC, real numbers are represented through weighted bitstreams, enabling complex arithmetic operations via streamlined distributions in the digital RTS sequence. This modulation bitwise logic on probabilistically encoded data streams. Critically, figure 4(c) confirms the output state ratio spans the range of 0–1, thereby satisfying the complete numerical range requirement for stochastic computational applications. Furthermore, as shown in figure 4(d), state ratio control at $T = 10$ K maintains identical trends to room-temperature operation. This demonstrates both the electrical control's wide-temperature versatility and its capacity for temperature compensation. Moreover, the results demonstrate tunability and robust operational margins as shown in figures 4(e) and (f). By adjusting either the amplitude or width of V_- or V_+, we also can control the proportion of '1's in the bitstream across the full range (0–1).

Stochastic computing finds foundational application in edge detection (ED). This technique employs convolutional kernels that process each image pixel to compute gradients, followed by adaptive

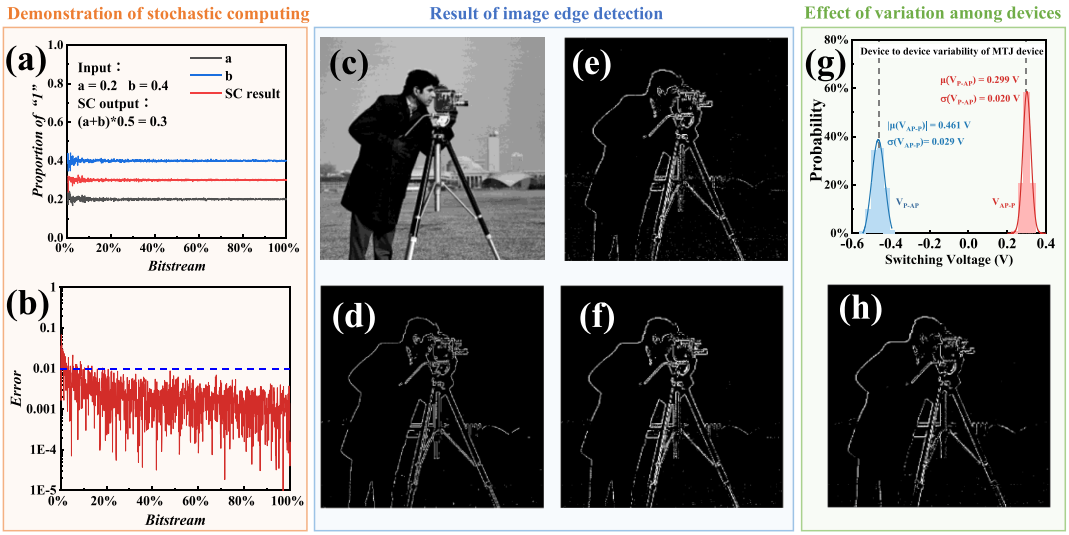

Figure 5. Edge detection results based on random calculations using RTS generator. (a) The convergence of SC results with respect to bitstream length (Inputs: $a = 0.2$, $b = 0.4$; theoretical output: 0.3). (b) The trend of calculation error decreasing with bitstream length. (c) The original image to be detected. (d) Edge detection results based on the MATLAB algorithm. Detection results when the bitstream length is 500 (e) and 1000 (f). (g) The V_{th} distribution among 200 devices. (h) The edge detection result when the input error is 10%.

thresholding for image edge extraction. The Roberts is used as a kernel in our study, which is one of the earliest ED operators and is represented by a 2 × 2 matrix.

Figure 4(g) presents the ED system implemented using the controllable RTS generator. Following grayscale conversion and normalization, pixel intensities are probabilistically encoded through the RTS generator based on MTJ, where '1' occurrence probability corresponds to grayscale values. The true random sequence representing the grayscale value matrix is processed through a multiplexer-based convolution to execute multiply–accumulate obtain the final ED result.

Figure 5(a) further illustrates the relationship between bitstream length and precision. It is observed that the method achieves high accuracy rapidly: with a bitstream length of only 1000 bits, the error is maintained within 1% in figure 5(b). Figure 5(c) depicts the original test image, while figure 5(d) displays the reference ED result obtained using MATLAB's edge function. The 500-bit random sequence implementation in figure 5(e) exhibits residual background artifacts and edge noise. Figure 5(f) demonstrates comparable accuracy to software algorithms at 1000-bit sequences. By modulating electrical parameters to rapidly generate value-specific true random sequences, this approach provides a low-power, compact hardware solution for compute-intensive operations like ED.

Besides, a statistical analysis of the device-to-device switching probability variation is important for practical applications. The threshold voltage (V_{th}) of 200 MTJ devices from the same wafer was measured. Figure 5(g) show that the V_{th} exhibits a very narrow Gaussian distribution in both the P → AP and AP → P directions. Their relative standard deviations (σ/μ) are only 6.3% and 6.7%, respectively. Then the performance of an image ED application was systematically simulated under varying degrees of variation. As shown in figure 5(h), even with an artificially introduced input error of 10% (exceeding the measured maximum relative deviation of 6.7%), the results show that core edge information remaining clearly visible due to the inherent error tolerance of stochastic computing [45].

3.3.3. RTS generator for artificial neural networks

Beyond serving as an entropy source for stochastic computation, the controllable RTS generator also play a key role in artificial neural networks. While prior studies indicate stochastic noise can mitigate neural network overfitting, physical noise sources typically lack extractability and tunability. The RTS generator addresses this limitation through enhanced randomness and modulation ability. As demonstrated in figure 6(a), we implement a long short-term memory networks (LSTM) for weather prediction with deliberately constrained training data (small training set/large validation set ratio) to simulate real-world data scarcity. Without intervention, figure 6(b) reveals classic overfitting: training error monotonically

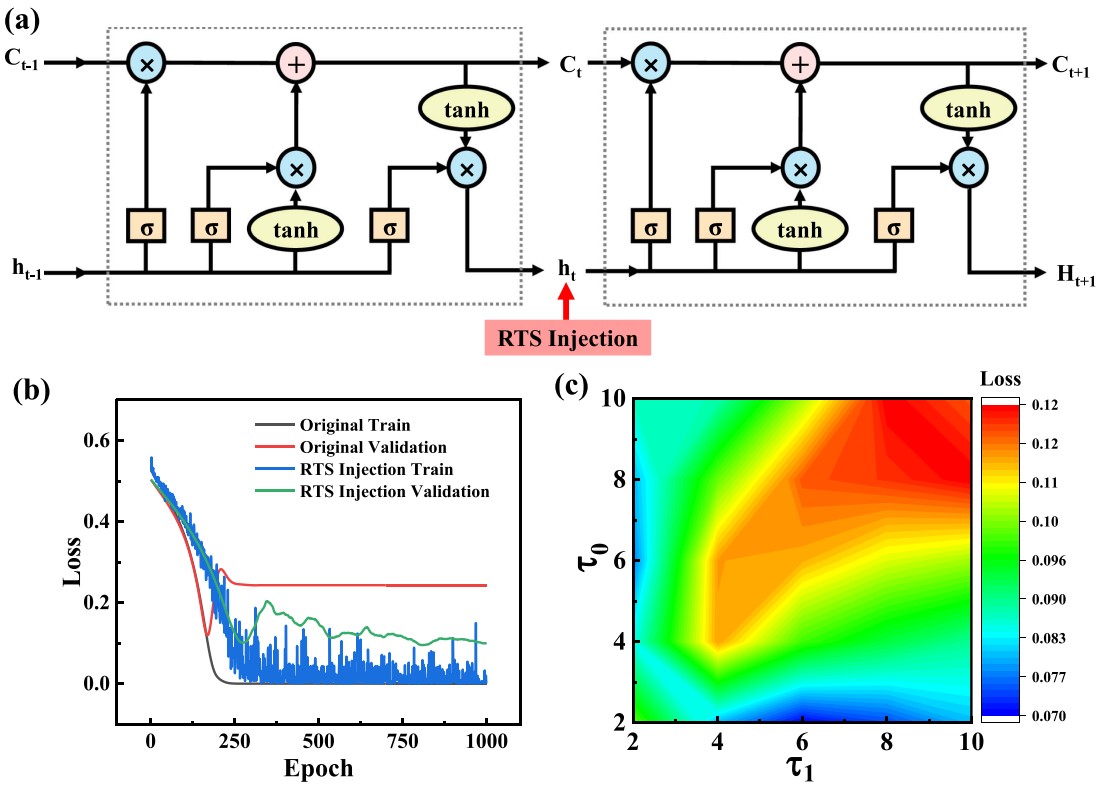

Figure 6. Demonstration of RTS generator in artificial neural network. (a) Architecture of noise injection in the hidden layer of LSTM. (b) Schematic diagram of LSTM overfitting state and training results after RTS injection. (c) Heat map of the relationship between verification error and time parameters (τ_0 and τ_1) of RTS signal.

decreases with epochs, while Injection of RTS into LSTM's hidden layer (figure 6(a)) significantly suppresses overfitting over 50%. Critically, figure 6(c) demonstrates time-parameter-dependent modulation of overfitting suppression—this controllability has the potential to further reduce the validation set error beyond what is currently possible.

4. Conclusion

This work establishes a voltage-driven spintronic RTS paradigm that overcomes fundamental limitations in entropy-source design. Existing RTS generation technologies have problems such as difficulty in extracting entropy sources and limited parameter control, which greatly restricts their practical applications as shown in table 1. In contrast, by exploiting electronic modulation within a single MTJ device, we demonstrate field-free RTS generation exhibiting cryptographic-grade randomness without external magnetic controls. The method enables dynamic parameter tuning of state occupation ratios (0–1) and transition time constants via excitation amplitude modulation, thereby facilitating adaptive stochastic computing. Validation across multiple domains confirms efficacy in secure communications (D–H protocols/voice encryption), edge detection, and machine learning (>50% overfitting suppression). This solution bridges intrinsic stochasticity with algorithmic requirements, establishing a new standard for secure, efficient intelligent hardware platforms.

Table 1. Comparison of RTS generation technologies.

	VLSI'16 [16]	VLSI'18 [20]	TED'19 [35]	SMACD' 25 [46]	TVLSI'17 [12]	This Work
Entropy Source	MOSFETs	MOSFETs	MTJ	MOSFETs	MOSFETs	MTJ
Entropy Source	Intrinsic gate oxide defects	Electrically stressed oxide traps	Thermally stable MTJ and external field	Intrinsic gate oxide defects	Intrinsic gate oxide defects	Voltage-controlled stochastic magnetization switching
Entropy extraction method	Screening of large device arrays	Electrical stress and dedicated AC operation	Magnetic field assistance	Need to find transistors with specific defects	Silicon Measurements	Fully electronic operation
NIST SP 800–22 tests result	Untested	9 tests passed	Untested	6–13 tests passed	9 tests passed	12 tests passed
Tunable parameters	None	Bit rate only	State dwell times (τ_{ap} and τ_{p})	Limited bit rate only	Bit rate only	State ratio (P(1)) and time constants ($\tau 0$, $\tau 1$)
Throughput	N/A	3 Mbps	∼1 kbps	N/A	∼100 bps	0.2–100 Mbps (Pulse-controlled)
Energy per bit	N/A	<1 pJ/bit	>10 nJ/bit	N/A	N/A	∼ 10 nJ/bit
Tuning mechanism	Not tunable	AC gate voltage and device stress	Dual bias: Voltage and magnetic field	Manual search	Gate voltage	Voltage amplitude only (V_+/V^-)
Key applications	Variability characterization	TRNG only	p-bit modeling	TRNG, PUF	TRNG	TRNG, SC, ANN

Data availability statement

All data that support the findings of this study are included within the article (and any supplementary files).

Acknowledgments

This work was financially supported by the National Key R&D Program of China (Grant No. 2025YFA1016400), the National Natural Science Foundation of China (Grant Nos. 62104188 and 12327806).

Conflict of interest

The authors declare no conflict of interest.

ORCID iDs

Zheng Chai 0000-0003-3446-7138
Xue Zhou 0000-0002-2218-0618
Xin Yue 0009-0008-0551-9203
Jian Fu Zhang 0000-0003-4987-6428
Weidong Zhang 0000-0003-4600-7382

References

[1] Picinbono B 2000 Moments and polyspectra of the discrete-time random telegraph signal *IEEE Trans. Inform. Theory* **46** 2735–9
[2] Chai Z *et al* 2020 GeSe-based ovonic threshold switching volatile true random number generator *IEEE Electron. Device Lett.* **41** 228–31
[3] Kwak M OTS-based analog-to-stochastic converter for fully-parallel weight update in cross-point array neural networks
[4] Locatelli N *et al* 2014 Noise-enhanced synchronization of stochastic magnetic oscillators *Phys. Rev. Appl.* **2** 034009
[5] Borders W A, Pervaiz A Z, Fukami S, Camsari K Y, Ohno H and Datta S 2019 Integer factorization using stochastic magnetic tunnel junctions *Nature* **573** 390–3
[6] Guo S *et al* 2018 Investigation on the amplitude coupling effect of random telegraph noise (RTN) in nanoscale FinFETs *2018 IEEE Int. Reliability Physics Symp. (IRPS)* (IEEE) pp P–TX.6–1–4
[7] Chou Y L, Wang T, Lin M, Chang Y W, Liu L, Huang S W, Tsai W J, Lu T C, Chen K C and Lu C-Y 2016 Poly-silicon trap position and pass voltage effects on RTN amplitude in a vertical NAND flash cell string *IEEE Electron. Device Lett.* **37** 998–1001
[8] Ma J, Chai Z, Zhang W, Govoreanu B, Zhang J F, Ji Z, Benbakhti B, Groeseneken G and Jurczak M 2016 Identify the critical regions and switching/failure mechanisms in non-filamentary RRAM (a-VMCO) by RTN and CVS techniques for memory window improvement *2016 IEEE Int. Electron Devices Meeting (IEDM)* (IEEE) pp 21.4.1–4
[9] Chai Z, Ma J, Zhang W, Govoreanu B, Simoen E, Zhang J F, Ji Z, Gao R, Groeseneken G and Jurczak M 2016 RTN-based defect tracking technique: experimentally probing the spatial and energy profile of the critical filament region and its correlation with HfO2RRAM switching operation and failure mechanism *2016 IEEE Symp. on VLSI Technology* (IEEE) pp 1–2
[10] Chen X, Wang L, Li B, Wang Y, Li X, Liu Y and Yang H 2016 Modeling random telegraph noise as a randomness source and its application in true random number generation *IEEE Trans. Comput.-Aided Des. Integr. Circuits Syst.* **35** 1435–48
[11] Brederlow R *et al* 2006 A low-power true random number generator using random telegraph noise of single oxide-traps *2006 IEEE Int. Solid State Circuits Conf.—Digest of Technical Papers* (IEEE) pp 1666–75
[12] Mohanty A, Sutaria K B, Awano H, Sato T and Cao Y 2017 RTN in scaled transistors for on-chip random seed generation *IEEE Trans. VLSI Syst.* **25** 2248–57
[13] Chai Z, Freitas P, Zhang W, Hatem F, Zhang J F, Marsland J, Govoreanu B, Goux L and Kar G S 2018 Impact of RTN on pattern recognition accuracy of RRAM-based synaptic neural network *IEEE Electron. Device Lett.* **39** 1652–5
[14] Puglisi F M, Zagni N, Larcher L and Pavan P 2018 Random telegraph noise in resistive random access memories: compact modeling and advanced circuit design *IEEE Trans. Electron Devices* **65** 2964–72
[15] Chang L-S, Huang C-Y, Tseng Y-H, King Y-C and Lin C-J 2013 Temperature sensing scheme through random telegraph noise in contact RRAM *IEEE Electron. Device Lett.* **34** 12–14
[16] Dongaonkar S, Giles M D, Kornfeld A, Grossnickle B and Yoon J 2016 Random telegraph noise (RTN) in 14nm logic technology: high volume data extraction and analysis *2016 IEEE Symp. on VLSI Technology* (IEEE) pp 1–2
[17] Tega N, Miki H, Ren Z, D'Emic C P, Zhu Y, Frank D J, Guillorn M A, Park D-G, Haensch W and Torii K 2011. Impact of HK/MG stacks and future device scaling on RTN. *2011 Int. Reliability Physics Symp. (IRPS)* (IEEE) p 6A.5.1–6A.5.6
[18] Chen C-Y, Ran Q, Cho H-J, Kerber A, Liu Y, Lin M-R and Dutton R W 2011 Correlation of Id- and Ig-random telegraph noise to positive bias temperature instability in scaled high-κ/metal gate n-type MOSFETs *2011 Int. Reliability Physics Symp. (IRPS)* (IEEE) p 3A.2.1–3A.2.6
[19] Guo S, Wang R, Mao D, Wang Y and Huang R 2017 Anomalous random telegraph noise in nanoscale transistors as direct evidence of two metastable states of oxide traps *Sci. Rep.* **7** 6239
[20] Brown J *et al* 2018 A low-power and high-speed true random number generator using generated RTN *2018 IEEE Symp. on VLSI Technology* (IEEE) pp 95–96
[21] Wong H-S P, Lee H-Y, Yu S, Chen Y-S, Wu Y, Chen P-S, Lee B, Chen F T and Tsai M-J 2012 Metal–Oxide RRAM *Proc. IEEE* **100** 1951–70
[22] Ielmini D 2016 Resistive switching memories based on metal oxides: mechanisms, reliability and scaling *Semicond. Sci. Technol.* **31** 063002
[23] Ielmini D and Wong H-S P 2018 In-memory computing with resistive switching devices *Nat. Electron.* **1** 333–43
[24] Beach R *et al* 2008. A statistical study of magnetic tunnel junctions for high-density spin torque transfer-MRAM (STT-MRAM) *2008 IEEE Int. Electron Devices Meeting (IEDM)* (IEEE) pp 1–4
[25] Dieny B *et al* 2020 Opportunities and challenges for spintronics in the microelectronics industry *Nat. Electron.* **3** 446–59
[26] Zhao H *et al* 2011 Low writing energy and sub nanosecond spin torque transfer switching of in-plane magnetic tunnel junction for spin torque transfer random access memory *J. Appl. Phys.* **109** 07C720
[27] Vodenicarevic D *et al* 2017 Low-energy truly random number generation with superparamagnetic tunnel junctions for unconventional computing *Phys. Rev. Appl.* **8** 054045
[28] Camsari K Y, Salahuddin S and Datta S 2017 Implementing p-bits With Embedded MTJ *IEEE Electron. Device Lett.* **38** 1767–70
[29] Shao Y, Sinaga S L, Sunmola I O, Borland A S, Carey M J, Katine J A, Lopez-Dominguez V and Amiri P K 2021 Implementation of artificial neural networks using magnetoresistive random-access memory-based stochastic computing units *IEEE Magn. Lett.* **12** 1–5
[30] Shao Y, Davila N, Ebrahimi F, Katine J A, Finocchio G and Khalili Amiri P 2023 Reconfigurable physically unclonable functions based on nanoscale voltage-controlled magnetic tunnel Junctions *Adv. Elect. Mater.* **9** 2300195
[31] Shao Y, Duffee C, Raimondo E, Davila N, Lopez-Dominguez V, Katine J A, Finocchio G and Khalili Amiri P 2023 Probabilistic computing with voltage-controlled dynamics in magnetic tunnel junctions *Nanotechnology* **34** 495203
[32] Finocchio G *et al* 2020 Spin–orbit torque based physical unclonable function *J. Appl. Phys.* **128** 033904
[33] Zhang J, Guo Z, Zhang S, Cao Z, Li R, Cao J, Song M, Wan M, Hong J and You L 2020 Spin–orbit torque-based reconfigurable physically unclonable functions *Appl. Phys. Lett.* **116** 192406
[34] Sato H, Yamanouchi M, Miura K, Ikeda S, Koizumi R, Matsukura F and Ohno H 2012 CoFeB thickness dependence of thermal stability factor in CoFeB/MgO perpendicular magnetic tunnel junctions *IEEE Magn. Lett.* **3** 3000204
[35] Zink B R, Lv Y and Wang J-P 2019 Independent control of antiparallel- and parallel-state thermal stability factors in magnetic tunnel junctions for telegraphic signals with two degrees of tunability *IEEE Trans. Electron Devices* **66** 5353–9
[36] Zink B R, Lv Y and Wang J-P 2018 Telegraphic switching signals by magnet tunnel junctions for neural spiking signals with high information capacity *J. Appl. Phys.* **124** 152121
[37] Yuan X, Jian J, Chai Z, An S, Gao Y, Zhou X, Zhang J F, Zhang W and Min T 2023 Markov chain signal generation based on single magnetic tunnel junction *IEEE Electron. Device Lett.* **44** 1963–6

[38] Yuan X, Chai Z, Zhou X, Luo Y, He Y, Jian J, Yue X, Zhang J F, Zhang W and Min T 2025 Hardware estimation for the eigenvectors of stochastic matrices using magnetic tunnel junctions *IEEE Electron. Device Lett.* **46** 500–3
[39] Igarashi J *et al* 2024 Single-nanometer CoFeB/MgO magnetic tunnel junctions with high-retention and high-speed capabilities *Npj Spintronics* **2** 1
[40] Heo S, Kim D, Choi W, Ban S, Kwon O and Hwang H 2023 Experimental demonstration of probabilistic-bit (p-bit) utilizing stochastic oscillation of threshold switch device *2023 IEEE Symp. on VLSI Technology and Circuits (VLSI Technology and Circuits)* (IEEE)pp 1–2
[41] Chai Z *et al* 2020 Stochastic computing based on volatile GeSe ovonic threshold switching selectors *IEEE Electron. Device Lett.* **41** 1496–9
[42] Liu B *et al* 2022 Bi_2 O_2 Se-based true random number generator for security applications *ACS Nano* **16** 6847–57
[43] Smith K J 2013 *Precalculus: A Functional Approach to Graphing and Problem Solving* (Jones & Bartlett Learning)
[44] Singhal A 2001 Modern information retrieval: a brief overview *IEEE Data Eng. Bull.* **24** 35–43 (available at: https://api.semanticscholar.org/CorpusID:260972090)
[45] Li P, Lilja D J, Qian W, Bazargan K and Riedel M D 2014 Computation on stochastic bit streams digital image processing case studies *IEEE Trans. VLSI Syst.* **22** 449–62
[46] Rubio-Barbero F J, De Los Santos-Prieto F, Castro-Lopez R, Roca E and Fernandez F V 2024 Harvesting RTN for true random number generators and physical unclonable functions *2024 20th Int. Conf. on Synthesis, Modeling, Analysis and Simulation Methods and Applications to Circuit Design (SMACD)* (IEEE) pp 1–4